The Astrophysical Journal, 855:21 (4pp), 2018 March 1 https://doi.org/10.3847/1538-4357/aaa7ef

Improved Ultraviolet and Infrared Oscillator Strengths for OH^+

James N. Hodges, Dror M. Bittner, and Peter F. Bernath
Department of Chemistry and Biochemistry, Old Dominion University, Norfolk, VA 23529, USA
Received 2017 November 8; revised 2018 January 10; accepted 2018 January 12; published 2018 February 28

Abstract

Molecular ions are key reaction intermediates in the interstellar medium. OH^+ plays a central role in the formation of more complex chemical species and for estimating the cosmic ray ionization rate in astrophysical environments. Here, we use a recent analysis of a laboratory spectrum in conjunction with ab initio methods to calculate infrared and ultraviolet oscillator strengths. These new oscillator strengths include branch dependent intensity corrections, arising from the Herman–Wallis effect, that have not been included before. We estimate 10% total uncertainty in the UV and 6% total uncertainty in the IR for the oscillator strengths.

Key words: astrochemistry – methods: laboratory: molecular – molecular data

Supporting material: machine-readable tables

1. Introduction

Molecular ions play a critical role in the chemical evolution of the interstellar medium (van Dishoeck & Black 1986; Le Petit et al. 2004) and as a means to probe physical conditions such as temperature and cosmic ray ionization rate (Porras et al. 2014; Hollenbach et al. 2012). One crucially important ion is OH^+. OH^+ is a step in the pathway to the formation of more complex oxygen and hydrogen containing species such as H_2O^+, H_3O^+, HO, and H_2O. Because all of this chemistry is dependent on cosmic ray ionization for initiation, it is critical that astronomers know cosmic ray ionization rates in various environments. Comparison of the column density of OH^+ to the total column density of hydrogen can be used to infer the cosmic ray ionization rate (Hollenbach et al. 2012; Porras et al. 2014; Indriolo et al. 2015). Therefore, detection and quantification of OH^+ column densities are a powerful tool for astronomers and astrophysicists.

The first detection of OH^+ in the interstellar medium occurred by Wyrowski et al. (2010). This detection was made in the submillimeter wave range toward Sagittarius B2(M). Shortly thereafter, Neufeld et al. (2010), Gerin et al. (2010), and González-Alfonso et al. (2013) made additional detections of OH^+ in the submillimeter range. The only other spectral range used to detect OH^+ is the UV (Krełowski et al. 2010; Porras et al. 2014; Bhatt & Cami 2015; Zhao et al. 2015). To the best of our knowledge, there have been no detections of OH^+ via the intense fundamental vibration near 3.3 μm.

Recent precise laboratory measurements of the fundamental mode (Markus et al. 2016) have spurred renewed efforts to improve the available line list of OH^+ in support of vibrational astronomical searches. We have analyzed near-UV spectra of the $A^3\Pi$–$X^3\Sigma^-$ band system, which were fit with the combined infrared and submillimeter measurements, to improve the predicted rest frequencies of the IR and UV transitions (Hodges & Bernath 2017).

We now present new calculations of oscillator strengths for the IR and UV lines. Using our improved spectroscopic constants, we have constructed empirical potential energy surfaces for the $A^3\Pi$ and $X^3\Sigma^-$ states, and we have calculated the transition and dipole moment functions using ab initio approaches. We have solved the radial Schödinger equation and used the wavefunctions and dipole moment function to determine the oscillator strengths of the IR and UV transitions.

These new values for the oscillator strengths are a marked improvement over values that have been determined previously (Gómez-Carrasco et al. 2014; Porras et al. 2014; Zhao et al. 2015) due to the use of an empirical potential energy surface, a higher level of ab initio theory to calculate the transition dipole moment function, and the inclusion of the "Herman–Wallis effect" (branch dependent intensity corrections to the rotational lines in a band).

With new values for oscillator strengths and transition frequencies, we can facilitate a better informed search in the IR and better quantify column densities in the UV. Making infrared measurements is important because they probe clouds with OH^+ column densities that are between the UV ($\sim 10^{12}\,cm^{-2}$) and the submillimeter ($\sim 10^{15}\,cm^{-2}$). For example, infrared H_3^+ measurements in diffuse clouds (Geballe & Oka 1996) and toward the Galactic Center (Oka et al. 2005) result in column densities on the order of $\sim 10^{14}\,cm^{-2}$. These new measurements will provide useful new observations in the IR and may help to characterize OH^+ in new interstellar environments.

2. Methodology

Empirical potential energy surfaces for the $A^3\Pi$ and $X^3\Sigma^-$ states were calculated by the Rydberg–Klein–Rees method using the program RKR1 by Le Roy (2017b). The equilibrium constants were taken from Hodges & Bernath (2017) and Merer et al. (1975) and are listed in Table 1.

The empirical potential energy surfaces are used as input to the program LEVEL by Le Roy (2017a). LEVEL also requires as input a dissociation energy and an energy offset between the two potential energy surfaces. The dissociation energy ($D_0 = 40270.2(2.9)\,cm^{-1}$) was determined using Active Thermochemical Tables (Ruscic 2015). The shift in energy is varied until the transition frequencies match Hodges & Bernath (2017). LEVEL solves the radial Schrödinger equation and can use a transition dipole moment function to calculate line strengths.

The ab initio transition dipole moment function is calculated with the MOLPRO quantum chemistry package (Werner et al. 2015). Transition moments and dipole moments have

Table 1
Equilibrium Constants

Constant	$X^3\Sigma^-$ (cm^{-1})	$A^3\Pi$ (cm^{-1})
ω_e	3119.2953(5)	2135.0782(54)
$\omega_e x_e$	83.1390(2)	79.55(1)[a]
$\omega_e y_e$	1.02792(3)	...
B_e	16.79484(1)	13.81265(23)
α_e	0.74903(1)	0.89174(19)
γ_e	0.010622(3)	0.01730(1)[a]

Note. Values in parenthesis are one standard deviation uncertainties. $X^3\Sigma^-$ constants are taken as is from Hodges & Bernath (2017) and $A^3\Pi$ values are fit with data from Hodges & Bernath (2017) using some fixed values from Merer et al. (1975).
[a] Fixed at value from Merer et al. (1975).

been calculated at the Multi-reference Configuration Interaction level of theory. The reference wavefunctions used were calculated at the state averaged Complete Active Space Self-consistent Field level of theory, employing the aug-cc-pV6Z basis sets. The state average included the $X^3\Sigma^-$, $1^1\Delta$, $1^3\Pi$, $1^1\Sigma^+$, $1^1\Pi$, $1^5\Sigma^-$, and $2^3\Sigma^-$ states, all having equal weights. These states have been used as they have been shown to give good results when using smaller basis sets and a smaller active space. The active space included the 2–7 σ-, 1–4 π-, and 1 δ-orbitals. The transition dipole moments were calculated on a grid of bond lengths with spacing 0.01 Å from 0.75 to 2.18 Å (Table 2) as expectation values.

LEVEL does not account for the effect of electron spin, so we include it in the same manner as Brooke et al. (2016) using a transformation equation to convert line strengths from Hund's "case b" to "case a" (Brown & Howard 1976). The transformed line strengths are input in the program PGOPHER, which calculates oscillator strengths and Einstein A coefficients (Western 2017).

3. Results and Conclusions

Following the procedure delineated in Section 2 and incorporating the constants reported by Hodges & Bernath (2017), an updated line list was generated for the $A^3\Pi$–$X^3\Sigma^-$ rovibronic transition (hereafter A–X) in the ultraviolet and the rovibrational transitions of the $X^3\Sigma^-$ ground state in the infrared (hereafter X–X). The calculated line list includes all experimentally observed vibrational levels (A, $v = 0$, 1; X, $v = 0$, 1, 2, 3, 4) up to $J'' = 30$. The line list with line positions, oscillator strengths, and Einstein A coefficients is presented in Table 3.

In order to assess the uncertainty on the calculated data sets, the potential energy surfaces are recalculated with $\pm 1\sigma$ of the values listed in Table 1, and the transition dipole moment function is shifted by ± 0.001 debye, the last significant figure. The significant figures for the transition dipoles are determined by adding an additional σ-orbital to the active space and checking the convergence of the transition dipole moment. The LEVEL calculations are run again with all combinations of potential energy surfaces and dipole moment functions. The differences between the maximum and minimum values of the line strengths are ratioed with the mean values to generate an error ratio for each line. The average ratio is then determined for the A–X transitions and ground state transitions. These are taken as the numerical precision of the calculations. For the

Table 2
Dipole Moments for the X–X and A–X Transitions as a Function of Bond Length

Bond Length (Å)	Dipole Moment X–X (D)	Dipole Moment A–X (D)
0.75	1.691	−0.516
0.76	1.709	−0.508
0.77	1.727	−0.501

(This table is available in its entirety in machine-readable form.)

A–X values, the average precision is 8%; for the ground state transitions, the average precision is 0.04%. The large discrepancy between the two data sets is likely due to the larger relative error on the transition dipole moment for the A–X data, and the $A^3\Pi$ state has fewer experimentally observed vibrational levels and is therefore more poorly determined.

These errors constitute just the precision of the calculations. The accuracy is more difficult to assess. It is worth noting that the Born–Oppenheimer approximation is less good with hydrides and the RKR approach relies on this approximation. To assess the accuracy, the A–X emission spectrum analyzed by Hodges & Bernath (2017) is compared to the calculated emission spectrum from PGOPHER. This is accomplished by checking the ratio of random experimental lines that share the same upper level to the same ratio from the calculated spectrum. The average percent error of these comparisons is 10%. This implies that the accuracy of the calculations is on average 6%, assuming the precision and accuracy uncertainties can be added in quadrature to generate the total uncertainty. Generally, the calculated spectrum matches the observed experimental spectrum very well, which can be seen in Figure 1. The uncertainties relative to experiment are similar to those calculated on the OH radical by Brooke et al. (2016). This calculation was performed in a similar manner to the calculation on OH^+, and it is reasonable that comparable uncertainties are achieved.

There are ~20 lines that have either been observed in the UV or expected to be astronomically relevant (refer to de Almeida & Singh 1981; Zhao et al. 2015). The oscillator strengths for the astronomical data are listed in Table 4. The data in Table 4 are presented as wavelengths in standard air using the updated index of refraction from Birch & Downs (1994) based on the work by Edlén (1966). The wavelengths are reproduced from Hodges & Bernath (2017). The most commonly observed transition is the feature at 3583.756 Å and the new oscillator strength is about a factor of two smaller than the recommended value from Porras et al. (2014) and used by Zhao et al. (2015). In fact, all of the oscillator strengths are smaller by about the same factor. The difference between the two data sets is that the band strength that Zhao et al. (2015) use (from Merchán et al. 1991) is larger than our own calculated band strength. Our ab initio calculation uses a more modern method to determine the transition dipole moment function and our potential energy surfaces are constructed with empirical methods, giving us greater confidence in our calculations. The very first calculation of oscillator strengths were performed by de Almeida & Singh (1981) using an empirical potential energy surface calculated by the Klein–Dunham procedure using the Merer et al. (1975) data and an experimental lifetime for the $A^3\Pi$ $v' = 0$. This lifetime was later shown to be too short. They used their potential energy surfaces to calculate Franck–Condon factors

Table 3
A Portion of the Line List with Positions, Oscillator Strengths, Lower State Energy, and Einstein A Coefficents

η'	v'	J'	N'	F_n' Parity	η''	v''	J''	N''	F_n'' Parity	Branch Label	Position (cm^{-1})	Position (Å)	f	E_{lower} (cm^{-1})	A (s^{-1})
X	1	1	0	F1e	X	0	0	1	F3e	pR13(0)	2926.0319	34175.977	1.59E-05	30.2832	30.20
X	1	1	2	F3e	X	0	0	1	F3e	rR3(0)	3019.2401	33120.917	2.99E-05	30.2832	60.60
X	1	1	0	F1e	X	0	1	1	F2f	pQ12(1)	2921.8971	34224.340	1.51E-05	34.418	85.82

Note. The table includes the upper (η') and lower electronic states (η''), as well as the upper and lower quantum numbers with each transition's appropriate branch label. The line position is reported as vacuum wavenumber and wavelength in standard air for the A–X transitions and vacuum wavelength for the X–X transitions.
(This table is available in its entirety in machine-readable form.)

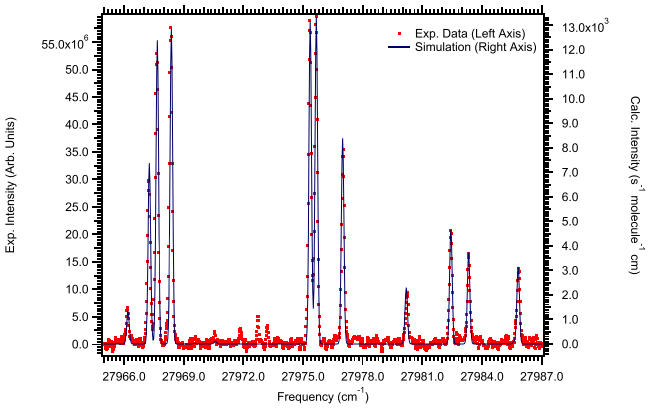

Figure 1. A portion of the experimental OH^+ emission spectrum analyzed by Hodges & Bernath (2017) plotted against a 1600 K simulation. The simulation shows excellent agreement with the laboratory data.

Table 4
A List of Astrophysically Relevant Transitions in Wavelength in Standard Air

Transition	Wavelength[a] (Å)	f (10^{-4})
(0, 0) $^qQ_{11}(1)$	3587.92650(16)	2.28
(0, 0) $^rR_{11}(0)$	3583.75574(16)	5.27
(0, 0) $^rR_{11}(1)$	3579.47011(15)	3.99
(0, 0) $^qQ_{22}(1)$	3577.133(12)	0.26
(0, 0) $^rQ_{21}(0)$	3572.65187(33)	3.12
(0, 0) $^rR_{22}(1)$	3570.6631(11)	1.08
(0, 0) $^sR_{21}(0)$	3566.4458(11)	1.17
(0, 0) $^rP_{31}(0)$	3565.34592(81)	1.28
(0, 0) $^sQ_{31}(0)$	3559.8062(13)	0.87
(0, 0) $^tR_{31}(0)$	3552.325(12)	0.05
(1, 0) $^qQ_{11}(1)$	3350.5956(15)	1.49
(1, 0) $^rR_{11}(0)$	3346.95559(74)	3.52
(1, 0) $^rR_{11}(1)$	3343.6395(10)	2.67
(1, 0) $^qQ_{22}(1)$	3341.223(11)	0.15
(1, 0) $^rQ_{21}(0)$	3337.3570(15)	2.06
(1, 0) $^rR_{22}(1)$	3335.959(11)	0.68
(1, 0) $^sR_{21}(0)$	3332.177(11)	0.82
(1, 0) $^rP_{31}(0)$	3330.409(11)	0.85
(1, 0) $^sQ_{31}(0)$	3326.369(11)	0.62
(1, 0) $^tR_{31}(0)$	3319.967(11)	0.04

Note. The transition labels in this table use the quantum number N in the parenthesis rather than J. This is done to match the labels published in other astronomical literature. This is discussed briefly in Hodges & Bernath (2017).
[a] Line positions from Hodges & Bernath (2017).

and r-centroids, which were used with the lifetime to calculate oscillator strengths. The measured lifetime was corrected by the experimental work of Möhlmann et al. (1978) and matched later theoretical calculations by Merchán et al. (1991) using Restricted Active Space Self-Consistent Field calculations to give reasonable agreement with experiment. These values were adopted by Porras et al. (2014) to provide a better estimate of the oscillator strengths and were recently used by Zhao et al. (2015) to estimate the band strengths of the (0, 0) and (1, 0) bands. Zhao et al. (2015) used the q_{00} Franck–Condon factor calculated by de Almeida & Singh (1981) and the intensity ratio of two lines from their observations to correct the q_{10} factor. All of this work is based on potential energy surfaces calculated with the 1975 spectroscopic data. Our updated spectroscopic measurements greatly improve the potentials on which we base our calculations. A recent ab initio calculation of by Gómez-Carrasco et al. (2014) calculates the dipole moment transition function with MOLPRO (Werner et al. 2015) but with many fewer active orbitals. They also rely on ab initio potential energy surfaces. Therefore, we expect our transition dipole moment and potential energy surfaces to be better. Moreover, we are the only calculation that treats the Herman–Wallis effect, which is strong for astrophysically relevant hydrides.

To validate our calculation, we calculate the radiative lifetime of the $A^3\Pi$ $v = 0$ level and compare it to the experimental value. Our radiative lifetime is 2.86 μs, which is in reasonable agreement with 2.5 $\pm$ 0.3 μs, the empirical value by Möhlmann et al. (1978). Moreover, the agreement with the high signal-to-noise laboratory spectrum presented in Hodges & Bernath (2017) (refer to Figure 1) gives added confidence in the quality of the calculations. As a test of the quality of our transition dipole moment function, we compare the intensity ratio of the $^rR_{11}(N'' = 0, J'' = 1)$ lines in the (0, 0) and (1, 0) bands as determined by Zhao et al. (2015) to the ratio of our calculated oscillator strengths. This ratio is an approximation of the ratio of the Franck–Condon factors. The ratio of our calculated oscillator strengths is within 6% error relative to Zhao et al. (2015), which is within our claimed uncertainty. This suggests that our transition dipole moment function has an accurate shape.

Regarding the infrared transitions, there is no reliable infrared intensity data so the the accuracy cannot be directly assessed. Conservatively, we can assign the same accuracy of 6% to the f-values of the infrared $X^3\Sigma^-$ state rovibrational transitions, though they likely are better given the differences between the two values of relative precision for the two data sets. These oscillator strengths are particularly important because, to the best of our knowledge, no astronomical observations have been made with the infrared transitions in the interstellar medium.

Overall, these calculations represent improved values for the oscillator strengths because they are the only calculations that

account for the Herman–Wallis effect. To assess the magnitude of this effect, we have calculated the line strengths with and without the Herman–Wallis effect, which is caused by a rotational dependence in the vibrational wavefunction (Bernath 2016). The Herman–Wallis effect is accounted for by LEVEL because it solves for the rovibrational wavefunction. In the infrared fundamental band, the P-branch is significantly stronger and the Herman–Wallis correction factor increases with lower rotational quantum number, J''. As an example, by $J'' = 10$, the values with versus without the inclusion of the Herman–Wallis effect differ by 80%. The magnitude of the Herman–Wallis effect in the UV transitions is not as pronounced. By $J'' = 15$, the data sets differ by 5%. We recommend that these *f*-values be used for the determination of column densities, as they represent a more accurate rotational dependence to the line strengths.

Support was provided by the NASA Laboratory Astrophysics program.

Software: RKR1 (Le Roy 2017b), LEVEL (Le Roy 2017a), MOLPRO (Werner et al. 2015), PGOPHER (Western 2017).

ORCID iDs

Dror M. Bittner https://orcid.org/0000-0002-4030-2797
Peter F. Bernath https://orcid.org/0000-0002-1255-396X

References

Bernath, P. F. 2016, in Spectra of Atoms and Molecules (3rd ed.; New York: Oxford Univ. Press), 10016
Bhatt, N. H., & Cami, J. 2015, ApJS, 216, 22
Birch, K. P., & Downs, M. J. 1994, Metro, 31, 315
Brooke, J. S., Bernath, P. F., Western, C. M., et al. 2016, JQSRT, 168, 142
Brown, J., & Howard, B. 1976, MolPh, 31, 1517
de Almeida, A. A., & Singh, P. D. 1981, A&A, 95, 383
Edlén, B. 1966, Metro, 2, 71
Geballe, T. R., & Oka, T. 1996, Natur, 384, 334
Gerin, M., De Luca, M., Black, J., et al. 2010, A&A, 518, L110
Gómez-Carrasco, S., Godard, B., Lique, F., et al. 2014, ApJ, 794, 33
González-Alfonso, E., Fischer, J., Bruderer, S., et al. 2013, A&A, 550, A25
Hodges, J. N., & Bernath, P. F. 2017, ApJ, 840, 81
Hollenbach, D., Kaufman, M. J., Neufeld, D., Wolfire, M., & Goicoechea, J. R. 2012, ApJ, 754, 105
Indriolo, N., Neufeld, D. A., Gerin, M., et al. 2015, ApJ, 800, 40
Krełowski, J., Beletsky, Y., & Galazutdinov, G. A. 2010, ApJL, 719, L20
Le Petit, F., Roueff, E., & Herbst, E. 2004, A&A, 417, 993
Le Roy, R. J. 2017a, JQSRT, 186, 167
Le Roy, R. J. 2017b, JQSRT, 186, 158
Linstrom, P. J., & Mallard, W. G. (ed.) 2017, NIST Chemistry WebBook, NIST Standard Reference Database Number 69 (Gaithersburg, MD: National Institute of Standards and Technology), doi:10.18434/T4D303
Markus, C. R., Hodges, J. N., Perry, A. J., et al. 2016, ApJ, 817, 138
Merchán, M., Malmqvist, P.-Å., & Roos, B. O. 1991, AcTC, 79, 81
Merer, A. J., Malm, D. N., Martin, R. W., Horani, M., & Rostas, J. 1975, CaJPh, 53, 251
Möhlmann, G., Bhutani, K., de Heer, F., & Tsurubuchi, S. 1978, CP, 31, 273
Moore, C. E. 1971, Atomic Energy Levels, Vol. 1 (Washington, DC: US Gov. Printing Office), 35
Neufeld, D. A., Goicoechea, J. R., Sonnentrucker, P., et al. 2010, A&A, 521, L10
Oka, T., Geballe, T. R., Goto, M., Usuda, T., & McCall, B. J. 2005, ApJ, 632, 882
Porras, A. J., Federman, S. R., Welty, D. E., & Ritchey, A. M. 2014, ApJL, 781, L8
Ruscic, B. 2015, JPCA, 119, 7810
van Dishoeck, E. F., & Black, J. H. 1986, APJS, 62, 109
Werner, H.-J., Knowles, P. J., Knizia, G., et al. 2015, MOLPRO, version 2015.1, A Package of Ab Initio Programs (Cardiff, UK), http://www.molpro.net
Western, C. M. 2017, JQSRT, 186, 221
Wyrowski, F., Menten, K. M., Güsten, R., & Belloche, A. 2010, A&A, 518, A26
Zhao, D., Galazutdinov, G. A., Linnartz, H., & Krełowski, J. 2015, ApJL, 805, L12